

# Stimulus-Specific Oscillations in a Retinal Model

Garrett T. Kenyon, Bryan J. Travis, James Theiler, John S. George, David W. Marshak

***Abstract*—** Evidence suggests that high frequency oscillatory potentials (HFOPs) in the vertebrate retina are stimulus-specific. The phase of the oscillation recorded at any given retinal location drifts randomly over time, but regions activated by the same stimulus remain phase locked with zero lag, whereas regions activated by separate stimuli become uncorrelated soon after stimulus onset. Based on retinal anatomy, we postulate that HFOPs are mediated by feedback from a class of axon-bearing amacrine cells that receive excitation from neighboring ganglion cells—via gap junctions—and make inhibitory synapses back onto the surrounding ganglion cells over a wide area. Using a computer model, we show that such circuitry can account for stimulus-specific HFOPs in response to both high- and low-contrast features. Phase locking between pairs of model ganglion cells did not depend critically on their separation distance, but on whether the applied stimulus created a continuous path between them. The degree of phase locking between separate stimuli was reduced by lateral inhibition, which created a buffer zone around strongly activated regions. As expected, stimulating this inhibited region increased the degree of phase locking proportionately. Our results suggest that stimulus-specific phase locking of retinal HFOPs results from a combination of local excitation and long-range inhibitory feedback.

### Acknowledgements

Manuscript received May 30, 2003. This work was supported in part by the National Eye Institute #EY06472, the National Institute of Neurological Disease and Stroke #NS38310, the Department of Energy Office of Nonproliferation Research and Engineering, the MIND Institute for Functional Brain Imaging, and by the Lab Directed Research and Development Program at LANL.

### Author Info

G. T. Kenyon is with the Los Alamos National Laboratory, P-21, MS D454, LANL, Los Alamos, NM 87545 USA (phone: 505-667-1900; fax: 505-665-4507; e-mail: [gkeyon@lanl.gov](mailto:gkeyon@lanl.gov)).

B. J. Travis is with the Los Alamos National Laboratory, EES-2, MS T003, LANL, Los Alamos, NM 87545 USA (phone: 505-667-1254; fax: 505-665-8737; e-mail: [bjtravis@lanl.gov](mailto:bjtravis@lanl.gov)).

J. Theiler is with the Los Alamos National Laboratory, NIS-2, MS B244, LANL, Los Alamos, NM 87545 USA (phone: 505-665-5682; fax: 505-665-4414; e-mail: [jt@lanl.gov](mailto:jt@lanl.gov)).

J. S. George is with the Los Alamos National Laboratory, P-21, MS D454, LANL, Los Alamos, NM 87545 USA (phone: 505-665-2550; fax: 505-665-4507; e-mail: [jsg@lanl.gov](mailto:jsg@lanl.gov)).

D. W. Marshak is with the Department of Neurobiology and Anatomy, University of Texas Medical School, Houston, TX 77030 USA (e-mail: [David.W.Marshak@uth.tmc.edu](mailto:David.W.Marshak@uth.tmc.edu)).

***Index Terms*— synchrony, gamma oscillations, phase locking, temporal code segmentation**

## I. INTRODUCTION

Ganglion cells — the output neurons of the retina — represent local stimulus properties, such as contrast, as changes in their firing rates. In addition, ganglion cells may encode global stimulus properties, such as connectedness, via coherent oscillations. Large stimuli can evoke high frequency oscillatory potentials (HFOPs) in mammalian retina at frequencies between 60-120 Hz [1-6], and similar oscillations have been recorded in cold-blooded vertebrates at lower frequencies [7, 8]. HFOPs are also present in electroretinograms (ERGs) of humans [9, 10] and other primates [11]. The phylogenetic conservation of HFOPs in vertebrate retina suggests they are important for visual function.

In those retinal preparations where the question of stimulus-specificity has been directly investigated, primarily in the frog [7] and cat [4], HFOPs were shown to be stimulus-specific. Oscillations arising from regions activated by the same contiguous stimulus were phase locked with zero lag, even though the phase itself varied randomly over time. In contrast, oscillations arising from regions activated by separate stimuli were temporally uncorrelated. The stimulus-specificity of retinal HFOPs suggests they encode global topological properties, such as connectedness. Compared to the visual cortex, where stimulus-specific oscillations have also been reported [12], the inner retina provides an ideal system for investigating how stimulus-specific HFOPs might arise from patterns of connectivity consistent with known anatomy and physiology.

In previous work using a linear retinal model, we proposed that negative feedback from axon-bearing amacrine cells—inhibitory inter-neurons—produced oscillatory responses that might underlie HFOPs [13]. According to this hypothesis, the dendrites of axon-bearing

amacrine cells are excited by neighboring ganglion cells via gap junctions and their axons provide feedback inhibition to more distant ganglion cells. This connectivity is consistent with patterns of ganglion cell tracer coupling [14-16], electron microscopy of gap junction contacts between ganglion and amacrine cells [15], and with the distribution of synaptic contacts made by wide-field amacrine cells [17, 18]. To investigate whether the HFOPs produced by axon-mediated feedback could be stimulus-specific, we developed a model of the inner retina, employing an integrate-and-fire process to describe the behavior of spiking neurons and a stochastic process to describe the effects of transmitter release from non-spiking neurons. Ganglion cells were modeled as cat alpha (Y) ganglion cells, based on physiological evidence that alpha ganglion cells fire synchronously [19, 20]. Preliminary reports of these results have appeared previously [21-23].

## II. METHODS

### A. Model Overview

The model retina consisted of five parallel, interconnected, 2-D grids, one for each cell type (fig. 1). Input to the model was conveyed by ON bipolar cells, which were driven by external currents representing light-modulated synaptic input from cone photoreceptors. These external currents were processed through a temporal low-pass filter with a time constant of 10 msec, but were not spatially filtered. The model bipolar cells produced excitatory postsynaptic potentials (EPSPs) in both ganglion cells and amacrine cells according to a random process [24]. EPSPs were balanced by inhibitory post-synaptic potentials, or IPSPs, from three different amacrine cell types encompassing three different spatial scales: 1) small amacrine cells that were the same size as the bipolar cells, 2) large amacrine cells that were the same size as the ganglion

cells, and 3) axon-bearing amacrine cells, whose widespread axonal connections excluded a small region around the center. Of the three amacrine cell types in the model, only the axon-bearing amacrine cells fired spikes. All three amacrine cell types made feedforward synapses onto ganglion cells, feedback synapses onto bipolar cells, as well as synapses among themselves.

### B. Simulation

All cell types were modeled as single compartment, RC circuit elements obeying a first order differential equation of the following form:

$$\dot{\vec{V}}^{(k)} = -\frac{1}{\tau^{(k)}} \left( \vec{V}^{(k)} - \vec{b}^{(k)} - \vec{L}^{(k)} - \sum_{k'} \vec{W}^{(k,k')} \cdot f^{(k,k')}(\vec{V}^{(k')}) \cdot \vec{W}^{(k,k')^T} \right), \quad (1)$$

where  $\{\vec{V}^{(k)}\}$  is a 2-D array denoting the normalized membrane potentials of all cells of type  $k$ ,  $1 \leq k \leq 5$ ,  $\tau^{(k)}$  are the time constants,  $\vec{b}^{(k)}$  are bias currents,  $\{\vec{L}^{(k)}\}$  are 2-D arrays representing light stimulation ( $\{\vec{L}^{(k)}\} = 0$ ,  $k \neq 1$ ),  $\{\vec{W}^{(k,k')}\}$  gives the connection strengths between presynaptic,  $k'$ , and postsynaptic,  $k$ , cell types as a function of their inter-row or inter-column separation and the functions  $f^{(k,k')}$  give the associated input-output relations, detailed below. The output of the axon-mediated inhibition was delayed by 2 msec, except for the axonal connections onto the axon-bearing amacrine cells, which was delayed for 1 msec. All other synaptic interactions were delayed by one time step, equal to 1 msec, representing a typical rise-time for PSPs. Equations were integrated using a direct Euler method. Separate control studies confirmed that the model exhibited similar behavior when a much smaller integration step was used, as long as the finite rise-times of PSPs were modeled explicitly.

The input-output function for gap junctions was given by the identity:

$$f^{(k,k')}(\vec{V}^{(k')}) = \vec{V}^{(k')}, \quad (2)$$

where the dependence on the presynaptic potential has been absorbed into the definition of  $\tau^{(k)}$ . The input-output function for non-spiking synapses was constructed by comparing, on each time step, a random number with a Fermi-function:

$$f^{(k,k')}(\tilde{V}^{(k')}) = \theta \left( \left[ \frac{1}{1 + \exp(-\alpha \tilde{V}^{(k')})} \right] - r \right), \quad (3)$$

where  $\alpha$  sets the gain (equal to 4 for all non-spiking synapses),  $r$  is a uniform random deviate equally likely to take any real value between 0 and 1, and  $\theta$  is a step function,  $\theta(x) = 1, x > 0$ ;  $\theta(x) = 0, x \leq 0$ .

Finally, the input-output relation used for spiking synapses was:

$$f^{(k,k')}(\tilde{V}^{(k')}) = \theta(\tilde{V}^{(k')}). \quad (4)$$

A modified integrate-and-fire mechanism was used to model spike generation. A positive pulse (amplitude = 10.0) was delivered to the cell on the time step after the membrane potential crossed threshold, followed by a negative pulse (amplitude = -10.0) on the subsequent time step. The bias current,  $b$ , was incremented by -0.5 following each spike, and then decayed back to the resting value with the time constant of the cell, thus implementing a relative refractory period.

Along both the horizontal and vertical directions, synaptic strengths fell off as Gaussian functions of the distance between the pre- and post-synaptic cells. For a given horizontal separation, the horizontal weight factor was determined by a Gaussian function of the following form:

$$W_{i^{(k)}, j^{(k')}}^{(k,k')} = \alpha \sqrt{W^{(k,k')}} e^{-\left[ \|i^{(k)} - j^{(k')}\|^2 / 2\sigma^2 \right]} \quad (5)$$

where  $\{W^{(k,k')}\}_{i^{(k)}, j^{(k' )}}$  is the horizontal weight factor from the presynaptic location  $j^{(k')}$  (the  $j^{\text{th}}$  column in the array of cells of type  $k'$ ) to the postsynaptic location  $i^{(k)}$  (the  $i^{\text{th}}$  column in the array of

cells of type  $k$ ),  $\alpha$  is a normalization factor, determined numerically, which ensured that the total integrated synaptic input equaled  $W^{(k,k)}$ ,  $\sigma$  is the Gaussian radius of the interaction, and the quantity  $\|i^{(k)} - j^{(k)}\|$  denotes the horizontal distance between the pre- and post-synaptic columns, taking into account the wrap around boundary conditions employed to mitigate edge effects. An analogous weight factor describes the dependence on the row separation. Equation 5 was augmented by a cutoff condition that prevents any synaptic interactions beyond a specified distance, determined by the radius of influence of the presynaptic outputs and the postsynaptic inputs, corresponding to the axonal and dendritic fields, respectively. A synaptic connection was only possible if the output radius of the presynaptic cell overlapped the input radius of the postsynaptic cell. Except for axonal connections, the input and output radii were the same for all cell types. For the large amacrine cells and the ganglion cells, the radius of influence extended out to the centers of the nearest neighboring cells of the same type. The radii of the bipolar, small, and axon-bearing amacrine cells (non-axonal connections only) extended only halfway to the nearest cell of the same type. The external input was multiplied by a gain factor of 3. Values for model parameters are listed in tables 1 and 2.

### *C. Data Analysis*

Cross-correlations between model ganglion cells were computed from pairs of binary spike trains and the result expressed as a fraction of the baseline synchrony (correlation amplitude at zero delay in the absence of a stimulus). The correlations between spike trains drawn from different stimulus trials (shift predictors) were used to estimate the contribution from stimulus coordination [25]. Correlations were plotted as a function of the delay after averaging over all events occurring during the plateau portion of the response (200-600 msec). For each delay value, this average was compensated for edge effects arising from the finite length of the two

spike trains. To increase the signal to noise, for some analyses it was advantageous to average over all cells, or distinct cell pairs, responding to the same stimulus, producing a multiunit Peri-Stimulus-Time-Histogram (mPSTH) or multi Cross-Correlation-Histogram (mCCH), respectively. Auto-correlation functions were not included in mCCH, which thus only included CCHs between distinct cell pairs. Error bars were estimated by assuming Poisson statistics for the count in each histogram bin. All rate and correlation measures, unless otherwise noted, were obtained by averaging over 200 stimulus trials, using a bin width of 1 msec. Distances within the model retina are reported in units of ganglion cell receptive field diameters, equivalent to the center-to-center separation between nearest neighbor pairs.

### III. RESULTS

#### A. HFOPs

A narrow bar centered over a column of eight model ganglion cells (fig. 2a) was used to simulate light responses. The response profile showing the plateau firing rate for each ganglion cell along a horizontal cross-section passing through the middle of the stimulus (fig. 2b<sub>1</sub>) was in qualitative agreement with the response profile predicted by a conventional Difference-of-Gaussians (DOG) model [26] (fig. 2b<sub>2</sub>). The surround radius of the equivalent DOG model was reduced by ~40% to accommodate the relatively small size of the model retinal circuit, but the relative center-surround strengths equaled published values. The mPSTH generated by the model exhibited a phasic-tonic profile typical of alpha ganglion cells (fig. 2c). The mPSTH was constructed using a small bin width (1 msec), allowing HFOPs during the response peak to be resolved. Similar HFOPs are evident during the initial portion of the PSTHs recorded from cat ganglion cells constructed using 1 msec bin widths [5], although in the experimental data the os-

cillations persisted longer into the response, probably due to the larger stimuli employed. Periodic structure is typically absent from the PSTHs of retinal ganglion cells, but this may reflect the use of large bins widths and/or temporal smoothing [27, 28], as well as the use of small centered spots or fine wavelength gratings that do not evoke HFOPs [1, 5, 7].

During the plateau portion of the response, HFOPs were clearly evident in the mCCH (fig. 2d, solid black line), obtained by combining the individual CCHs of all distinct pairs of ganglion cells activated by the stimulus. The CCH measures the joint firing probability of cell pairs as a function of the time delay between their two spikes, with the results expressed here as a fraction of the expected synchrony due to chance. The oscillation frequency, the relative magnitude of the central correlation peak, and the persistence of the firing correlations between the model ganglion cells, were similar to their corresponding experimentally observed values [4].

Oscillatory activity was not evident during the plateau portion of the mPSTH, since the phases of retinal HFOPs are not stimulus-locked but instead drift randomly over time, and thus tend to average out over multiple trials. Due to the ongoing random drift in the phase of the HFOPs, the correlation amplitude fell off as a function of increasing delay, as indicated by the reduced height of successive side peaks in the mCCH. When spike trains were drawn from separate stimulus trials, in order to estimate correlations due to stimulus coordination, the shift predictor was negligible (fig. 2d, dashed gray line). Unless otherwise noted, all CCHs presented in this study included only the residual firing correlations between distinct cells pairs after the shift predictor had been subtracted.

HFOPs produced by the same stimulus could remain phase locked over considerable distances. CCHs were evaluated for ganglion cell pairs arranged symmetrically about the center of a narrow bar (fig. 3) using data from the plateau portion of the response. Regardless of whether

correlations were measured between cell pairs separated by small, intermediate or large numbers of receptive field diameters, prominent phase locked oscillations were always clearly evident in the CCHs.

### *B. Stimulus-Specificity*

Phase locking of HFOPs in the retinal model was stimulus-specific. We examined the HFOPs evoked by two identical bars that were turned on simultaneously (fig. 4a). HFOPs were phase locked between regions responding to the same bar, but not between locations responding to different bars. CCHs obtained during the plateau portion of the response were plotted for ganglion cell pairs at opposite ends of the same bar (fig. 4b<sub>1</sub>, upper bar; fig. 4b<sub>3</sub>, lower bar), or at the nearest opposing tips of the two separate bars (fig. 4b<sub>2</sub>). Even though the ganglion cells in each pair were separated by the same distance and were stimulated identically within their receptive field centers, only HFOPs within the same bar were strongly phase locked.

The degree of phase locking between the HFOPs evoked by separate stimuli was examined systematically as a function of the distance separating two identical bars aligned end-to-end (fig. 5). As measured by the CCHs between a fixed pair of model ganglion cells, HFOPs at the two recording sites were substantially phase locked when the opposing tips of the two bars were separated by a distance less than the diameter of a ganglion cell receptive field, but became largely independent at greater separations. Ganglion cells between the two stimuli were strongly suppressed by lateral inhibition and thus did not fire spikes, as shown by the spatial profile of the plateau firing rates along a vertical cross section passing down the central axis of the two stimuli. However, phase information could still be communicated between closely spaced stimuli via gap junctions. The sharp fall off in phase locking with increasing separation is consistent with a dependence on gap junctions, which necessarily only link nearest neighbors. In contrast, the long

range of axon-mediated inhibition interactions is incommensurate with a sharp dependence on separation distance.

The degree of phase locking between HFOPs evoked by separate bars was proportional to the activity of the neurons in the space between them. CCHs were recorded between a pair of ganglion cells responding to two separate bars while the cells in the region between them were stimulated at a lower or equal intensity (fig. 6). Phase locking between HFOPs recorded at the two sites increased in proportion to the intensity of the stimulation in the connecting region. Phase locking between the two bars remained substantial as long as the stimulus intensity in the connecting region was at or above approximately  $\frac{1}{4}$  the intensity of the two bars. The spatial profile of the plateau firing rate along a vertical cross-section passing through the main axis of the two stimuli revealed a relationship between the activity of the ganglion cells in the connecting region and the degree of phase locking between the two bars. HFOPs evoked by the two bars were mostly phase independent as long as the activity of the ganglion cells in the connecting region was below baseline levels. Axon-mediated interactions directly between the two bars were not sufficient, by themselves, to promote strong phase locking. Instead, phase locking between distant sites had to be established, at least in part, through a series of nearest-neighbor steps via gap junctions.

To investigate the phase locking of HFOPs in continuously shaded regions, the intensity along a narrow bar was modulated in a sinusoidal fashion, thus producing two patches of elevated intensity in the absence of any abrupt high-contrast borders along the stimulus axis (fig. 7). CCHs were computed between pairs of ganglion cells located at four equidistant points, chosen such that the local intensity within their receptive field centers equaled the average intensity over one cycle of the stimulus (half way between the maximum and minimum values). HFOPs were

stimulus-specific even for relatively shallow intensity modulations and become progressively more so as the modulation depth increased. Thus, along a narrow contour, the phase locking behavior of model-generated HFOPs showed the same stimulus-specificity for features defined by shaded boundaries as has been previously reported for features defined by sharp borders.

#### IV. DISCUSSION

##### *A. Stimulus-Selective HFOPs from Retinal Circuitry*

HFOPs are ubiquitous in the vertebrate retina. One clue to their function is the strong stimulus-specificity exhibited by HFOPs recorded simultaneously at separate retinal locations. Here, we have used a computer model to explore the circuitry underlying the phase locking behavior of retinal HFOPs. While it is not currently practical to model a system as complex as the mammalian retina to an arbitrary degree of physiological accuracy, a computational approach is nonetheless a potentially useful way to investigate functional relationships between anatomy and physiology. In particular, a computational model can determine whether connectivity consistent with known anatomy is sufficient to account for a given set of physiological behaviors. We have explored the phase locking behavior of HFOPs produced by patterns of synaptic connectivity found in the inner retina. Our results demonstrate that inhibitory feedback from axon-bearing amacrine cells, themselves electrically coupled to ganglion cells, could account for the known phase locking behavior of retinal HFOPs. HFOPs produced by axon-mediated feedback were of the same general frequency, amplitude, and duration—as measured by the persistence of side-peaks in the CCH—as HFOPs recorded experimentally. Our results suggest that retinal patterns of connectivity may be specifically organized so that HFOPs are most strongly phase locked between connected regions responding to the same stimulus.

Model generated HFOPs recorded at separate retinal locations were phase locked whenever there was a continuous path of stimulated cells joining them. This finding suggests that the one topological parameter encoded by phase locked HFOPs is connectedness. In principle, topological information encoded by the degree of phase locking between retinal HFOPs could be read out by downstream neurons. For example, HFOPs arising from simply connected regions of the visual space would add in phase, and thus might produce larger responses than HFOPs arising from non-connected regions, which would add with random phase. Sensitivity to synchronous input has been demonstrated in visual cortical neurons [29], suggesting that retinal HFOPs might contribute to the detection of contiguous features. Retinal HFOPs may also influence the development of intra-cortical connections via spike-timing-dependent-plasticity (STDP) [30]. By causing regions responding to the same object to oscillate in phase, retinal HFOPs may contribute to the development of appropriate feature detectors in the visual cortex.

Retinal circuitry gave rise to HFOPs that were always at least partially stimulus-specific. When bar stimuli were moved apart by more than one ganglion cell receptive field center diameter, their HFOPs were no longer appreciably phase locked, even at separations for which there would still have been many long range axonal fibers crossing between them. In other experiments, it was shown that the degree of phase locking between separate bar stimuli depended directly on stimulation of the intervening cells. The ability to modulate the degree of phase locking between fixed objects whose axon-mediated interconnections were unchanged, highlights the dependence of phase locking on local interactions, particularly gap junctions. Previous theoretical work has demonstrated that gap junctions, due to their low pass temporal filter characteristics, cause action potentials to be strongly attenuated [13]. Thus, spikes cannot be passively propagated through chains of gap junctions, and instead must be boosted by firing events along the way to be reliably

transmitted. Due to lateral inhibition, separate stimuli tend to be surrounded by halos of suppressed activity, which in turn act to block the propagation of spikes through the chains of gap junctions. This block can be relieved, however, by stimulating the intervening cells sufficiently to bring them near threshold. Here, a sufficiently level of firing for propagating phase information through local connections was on the order of the background activity.

Two very different synaptic mechanisms contributed to the phase locking of HFOPs in the retinal model. While axon-mediated feedback was necessary to establish an oscillatory rhythm, local interactions, and in particular gap junctions, were critical for locking the phases of neighboring cells. These two complementary synaptic mechanisms, acting in concert, are predicted to produce the stimulus-selective phase locking behavior of retinal HFOPs. Given the high level of synaptic noise in the retinal model, the phase locking behavior exhibited by these two synaptic mechanisms is likely to be robust, and thus the principal characteristics of phase locking behavior exhibited by the present retinal model should not depend on the precise details of the implementation.

### *B. Physiological Evidence*

Many of the assumptions made in our retinal model are consistent with physiological and anatomical studies in both cats and primates. When both alpha ganglion cells in the cat and parasol ganglion cells in the primate are filled with neurobiotin, at least two distinct amacrine cell types are labeled, one that gives rise to long axons as well as one or more conventional cell types [14-16]. The observed patterns of tracer coupling are consistent with our assumption that ganglion cells are directly coupled to the axon-bearing amacrine cells and that the axon-bearing amacrine cells are also tracer-coupled to each other [16]. Furthermore, the synaptic interactions of morphologically similar amacrine cell types [31] are consistent with our assumption that the

major excitatory input to the axon-bearing amacrine cells was from electrical synapses and that their outputs were directed to bipolar, amacrine, and ganglion cells, including alpha ganglion cells [18, 32]. Approximately 80% of all synapses onto either alpha ganglion cells or primate parasol cells are from amacrine cells [15, 17], consistent with our assumption that amacrine cell inputs play a major role in shaping ganglion cell light responses. Finally, the serial connectivity between the three amacrine cell types in the model is consistent with anatomical evidence for serial inhibition between amacrine cells [33]. Negative feedback from such serial interactions allowed the three different amacrine cell types in the model to regulate each other, thereby increasing the dynamic range of ganglion cell responses.

#### REFERENCES:

1. Ariel, M., N.W. Daw, and R.K. Rader, *Rhythmicity in rabbit retinal ganglion cell responses*. Vision Research, 1983. **23**(12): p. 1485-93.
2. Frishman, L.J., et al., *Spatiotemporal frequency responses of cat retinal ganglion cells*. Journal of General Physiology, 1987. **89**(4): p. 599-628.
3. Laufer, M. and M. Verzeano, *Periodic activity in the visual system of the cat*. Vision Res, 1967. **7**(3): p. 215-29.
4. Neuenschwander, S. and W. Singer, *Long-range synchronization of oscillatory light responses in the cat retina and lateral geniculate nucleus*. Nature, 1996. **379**(6567): p. 728-32.
5. Neuenschwander, S., M. Castelo-Branco, and W. Singer, *Synchronous oscillations in the cat retina*. Vision Res, 1999. **39**(15): p. 2485-97.
6. Steinberg, R.H., *Oscillatory activity in the optic tract of cat and light adaptation*. J Neurophysiol, 1966. **29**(2): p. 139-56.

7. Ishikane, H., A. Kawana, and M. Tachibana, *Short- and long-range synchronous activities in dimming detectors of the frog retina*. Vis Neurosci, 1999. **16**(6): p. 1001-14.
8. Wachtmeister, L. and J.E. Dowling, *The oscillatory potentials of the mudpuppy retina*. Invest Ophthalmol Vis Sci, 1978. **17**(12): p. 1176-88.
9. Wachtmeister, L., *Oscillatory potentials in the retina: what do they reveal*. Prog Retin Eye Res, 1998. **17**(4): p. 485-521.
10. De Carli, F., et al., *Stimulus- and frequency-specific oscillatory mass responses to visual stimulation in man*. Clin Electroencephalogr, 2001. **32**(3): p. 145-51.
11. Frishman, L.J., et al., *Effects of experimental glaucoma in macaques on the multifocal ERG. Multifocal ERG in laser-induced glaucoma*. Doc Ophthalmol, 2000. **100**(2-3): p. 231-51.
12. Gray, C.M., et al., *Oscillatory responses in cat visual cortex exhibit inter-columnar synchronization which reflects global stimulus properties*. Nature, 1989. **338**(6213): p. 334-7.
13. Kenyon, G.T. and D.W. Marshak, *Gap junctions with amacrine cells provide a feedback pathway for ganglion cells within the retina*. Proc R Soc Lond B Biol Sci, 1998. **265**(1399): p. 919-25.
14. Dacey, D.M. and S. Brace, *A coupled network for parasol but not midget ganglion cells in the primate retina*. Visual Neuroscience, 1992. **9**(3-4): p. 279-90.
15. Jacoby, R., et al., *Synaptic inputs to ON parasol ganglion cells in the primate retina*. Journal of Neuroscience, 1996. **16**(24): p. 8041-56.
16. Vaney, D.I., *Patterns of neuronal coupling in the retina*. Progress in Retinal and Eye Research, 1994. **13**: p. 301-355.
17. Freed, M.A. and P. Sterling, *The ON-alpha ganglion cell of the cat retina and its presynaptic cell types*. Journal of Neuroscience, 1988. **8**(7): p. 2303-20.

18. Kolb, H. and R. Nelson, *OFF-alpha and OFF-beta ganglion cells in cat retina: II. Neural circuitry as revealed by electron microscopy of HRP stains*. Journal of Comparative Neurology, 1993. **329**(1): p. 85-110.
19. Castelo-Branco, M., S. Neuenschwander, and W. Singer, *Synchronization of visual responses between the cortex, lateral geniculate nucleus, and retina in the anesthetized cat*. J Neurosci, 1998. **18**(16): p. 6395-410.
20. Mastronarde, D.N., *Correlated firing of retinal ganglion cells*. Trends in Neurosciences, 1989. **12**(2): p. 75-80.
21. Kenyon, G.T., K.R. Moore, and D.W. Marshak, *Stimulus-specific synchrony between alpha ganglion cells in a computer model of the mammalian retina*. Society for Neuroscience, 1999. **25**: p. 1042.
22. Kenyon, G.T. and D.W. Marshak, *Synchrony of ganglion cells encodes stimulus intensity in a retinal model*. Society for Neuroscience, 2000. **26**: p. 1328.
23. Kenyon, G.T. and D.W. Marshak, *Amacrine cells synchronize the firing of alpha ganglion cells over a wide range of stimulus intensities*. IVOS, 2001. **42**(4): p. S674.
24. Freed, M.A., *Rate of quantal excitation to a retinal ganglion cell evoked by sensory input*. J Neurophysiol, 2000. **83**(5): p. 2956-66.
25. Gerstein, G.L. and D.H. Perkel, *Mutual temporal relationships among neuronal spike trains. Statistical techniques for display and analysis*. Biophys J, 1972. **12**(5): p. 453-73.
26. Troy, J.B., J.K. Oh, and C. Enroth-Cugell, *Effect of ambient illumination on the spatial properties of the center and surround of Y-cell receptive fields*. Visual Neuroscience, 1993. **10**(4): p. 753-64.

27. Cox, J.F. and M.H. Rowe, *Linear and nonlinear contributions to step responses in cat retinal ganglion cells*. Vision Research, 1996. **36**(14): p. 2047-60.
28. Enroth-Cugell, C. and H.G. Jakiela, *Suppression of cat retinal ganglion cell responses by moving patterns*. Journal of Physiology, 1980. **302**: p. 49-72.
29. Alonso, J.M., W.M. Usrey, and R.C. Reid, *Precisely correlated firing in cells of the lateral geniculate nucleus*. Nature, 1996. **383**(6603): p. 815-9.
30. Yao, H. and Y. Dan, *Stimulus timing-dependent plasticity in cortical processing of orientation*. Neuron, 2001. **32**(2): p. 315-23.
31. Vaney, D.I., L. Peichl, and B.B. Boycott, *Neurofibrillar long-range amacrine cells in mammalian retinae*. Proceedings of the Royal Society of London - Series B: Biological Sciences, 1988. **235**(1280): p. 203-19.
32. Freed, M.A., et al., *ON-OFF amacrine cells in cat retina*. Journal of Comparative Neurology, 1996. **364**(3): p. 556-566.
33. Marc, R.E. and W. Liu, *Fundamental GABAergic amacrine cell circuitries in the retina: nested feedback, concatenated inhibition, and axosomatic synapses*. J Comp Neurol, 2000. **425**(4): p. 560-82.

TABLE I  
CELLULAR PARAMETERS

	$\tau$	$b$	$n \times n$	$d$	$\sigma$
<b>BP</b>	10.0	-0.0	64×64	0.25	0.25
<b>SA</b>	25.0	-0.5	64×64	0.25	0.25
<b>LA</b>	20.0	-0.25	32×32	1.0	0.5
<b>PA</b>	5.0	-0.025	64×64	0.25/9.0 <sup>a</sup>	0.25/3.0 <sup>a</sup>
<b>GC</b>	5.0	-0.025	32×32	1.0	0.5

Explanation of symbols:  $\tau$ : time constant (msec);  $b$ : bias;  $n \times n$ : array size;  $d$ : cutoff radius,  $\sigma$ : Gaussian radius (see eq. 5). <sup>a</sup>Inner radius/outer radius.

TABLE 2  
SYNAPTIC WEIGHTS

	BP	SA	LA	PA	GC
BP	*	-0.375 <sup>b</sup>	3.0 <sup>b</sup>	-3.0 <sup>b</sup> /-15.0 <sup>c</sup>	*
SA	3.0 <sup>b</sup>	*	-3.0 <sup>b</sup>	0.0 <sup>b</sup> /-15.0 <sup>c</sup>	*
LA	3.0 <sup>b</sup>	*	0.25 <sup>a</sup>	-3.0 <sup>a</sup> /-15.0 <sup>c</sup>	*
PA	0.75 <sup>b</sup>	-0.75 <sup>b</sup>	0.25 <sup>a</sup>	0.25 <sup>a</sup> /-45.0 <sup>c</sup>	0.25 <sup>a,d</sup>
GC	9.0 <sup>b</sup>	-4.5 <sup>b</sup>	-4.5 <sup>b</sup>	0.25 <sup>a</sup> /-270.0 <sup>c</sup>	*

Each term represents the total integrated weight from all synapses arising from the corresponding presynaptic type (columns) to each cell of the corresponding postsynaptic type (rows), (the quantity  $W^{(i,i')}$  in eq. 5). Asterisk (\*) indicates absence of corresponding connection. Synapse type indicated by superscript: <sup>a</sup>gap junction, <sup>b</sup>non-spiking synapse, <sup>c</sup>spiking synapse. <sup>d</sup>Maximum coupling efficiency (ratio of post- to pre-synaptic depolarization) for this gap junction synapse: DC=11.3%, Action Potential=2.7%.

## Figure Captions

Fig. 1. Major types of connections in the retinal model. The model contained five cells types: bipolar (BP) cells, small (SA), large (LA) and poly-axonal (PA) amacrine cells, and alpha ganglion (GC) cells. All three circuits produced negative feedback, but only axon-mediated feedback produced HFOPs. Explanation of symbols: Excitation (triangles), inhibition (circles), gap junctions (resistors).

Fig. 2. Stimulus-evoked HFOPs. a) Column of eight model ganglion cells stimulated by a narrow bar (intensity =  $\frac{1}{2}$ ). b<sub>1</sub>) Plateau firing rates of ganglion cells along horizontal cross-section through the center of the stimulus (intensity =  $\frac{1}{16}$ ). b<sub>2</sub>) Response profile predicted by a difference-of-Gaussians (DOG) model. c) mPSTH. Solid line indicates the stimulus duration. Vertical ticks denote the peak and plateau portions of the response (bin width, 1 msec). d) Solid black line: mCCH. Dashed gray line: Shift predictor. Only the time varying component of the shift predictor is plotted. Ganglion cells are synchronized by a fast oscillation (95 Hz) that is not phase locked to the stimulus onset.

Fig. 3. HFOPs decline gradually with distance. a) CCHs between ganglion cell pairs arranged symmetrically about the center of a bar stimulus. Center-to-center distance (dist) shown to upper right corner of each plot.

Fig. 4. HFOPs are stimulus-selective for high contrast features. a) Location of stimuli (white rectangles) relative to the receptive field centers of recorded ganglion cells, labeled 1-4 (circles). b<sub>1</sub>-b<sub>3</sub>) CCHs (solid black lines) and associated shift predictors (dashed gray lines) computed during the plateau portion of the response for pairs of ganglion cells at opposite ends of the same bar

or at opposing tips of separate bars. All ganglion cell pairs were separated by 7 GC receptive field diameters. b<sub>1</sub>) pair 1↔2 from upper bar; b<sub>2</sub>) pair 2↔3 from separate bars; b<sub>3</sub>) pair 3↔4 from lower bar. Correlations were only significant between pairs from the same bar.

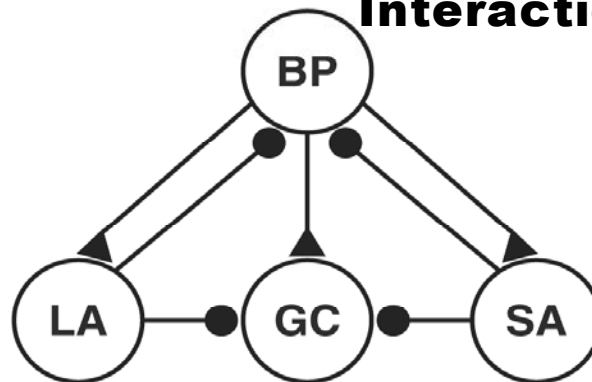
Fig. 5. Phase locking of HFOPs declines rapidly as the separation distance increases. Left column: Plateau CCHs between a fixed pair of ganglion cells responding to two separate bars. The distance between the opposing ends of the two bars (gap) is indicated in the upper-right of each plot. Correlations fall off rapidly with increasing separation. Right column: Spatial profile of the plateau firing rate along a cross-section through the central axis of the two stimuli. The plateau firing rates of the cells in the gap are very nearly zero.

Fig. 6. Phase-locking of HFOPs is proportional to the activity between stimuli. Left column: Plateau CCHs (solid black lines) and associated shift-predictors (dashed gray lines) between a fixed pair of ganglion cells stimulated by two separate bars. The intensity of both bars was  $-1$  ( $\log_2$  units) while cells in the gap between them were stimulated at an equal or lower intensity, indicated to the upper right of each plot. Phase locking between stimuli increase with gap intensity. Right column: Spatial profile of plateau firing activity along a cross section through the principal axis of the two stimuli. The firing rate of ganglion cells in the gap is above or near baseline levels when stimulated by an intensity greater than approximately  $\frac{1}{4}$  that of the bars themselves, consistent with the gap intensity below which firing correlations become very weak.

Fig. 7. Firing correlations can group features defined by shaded boundaries. a) Top: Sinusoidally modulating the intensity of a narrow bar produces two distinct patches. Middle: Cross-

section of stimulus intensity profile. Bottom: Plateau firing rates of cells along the axis of the bar stimulus. Arrows indicate the locations of 4 symmetrically placed cells that received similar center stimulation. b) CCFs between cell pairs denoted in denoted in panel a. Cells responding to the same patch were more strongly correlated than cells responding to different patches. c,d) Same organization as in a,b) except the depth of the sinusoidal modulation was increased, causing the firing correlations to become even more feature selective.

### A. Feedforward & Feedback Interactions



### B. Serial Interactions



### C. Oscillatory Interactions

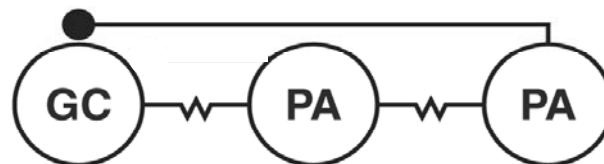


Figure 1

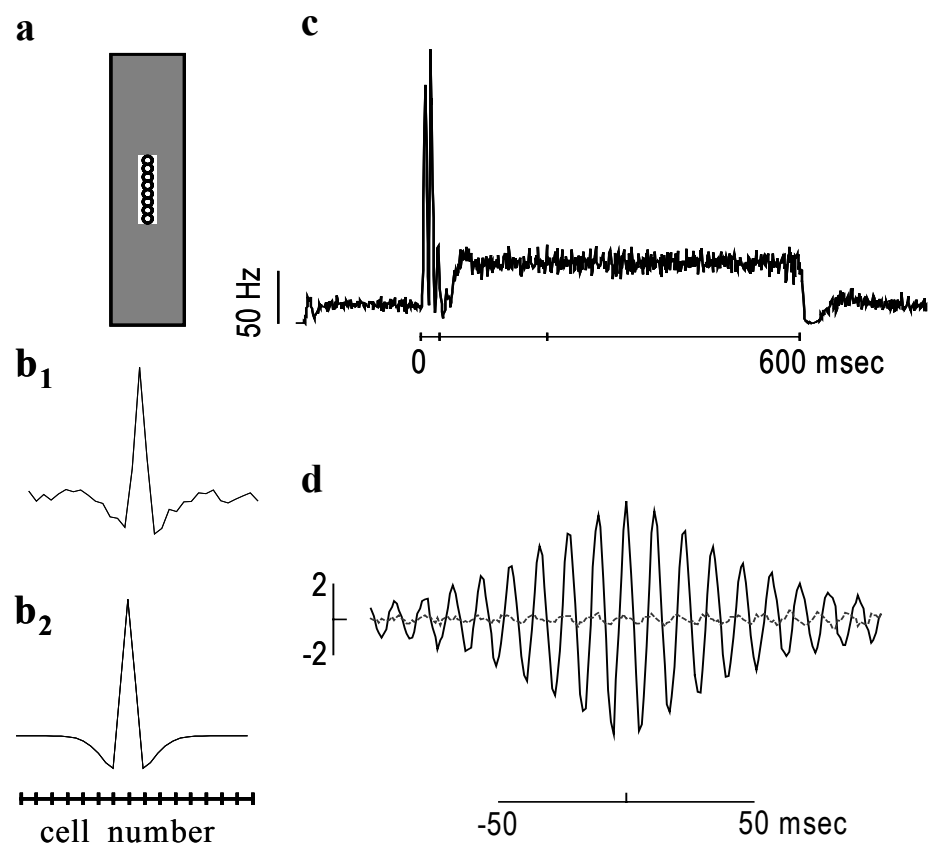


Figure 2

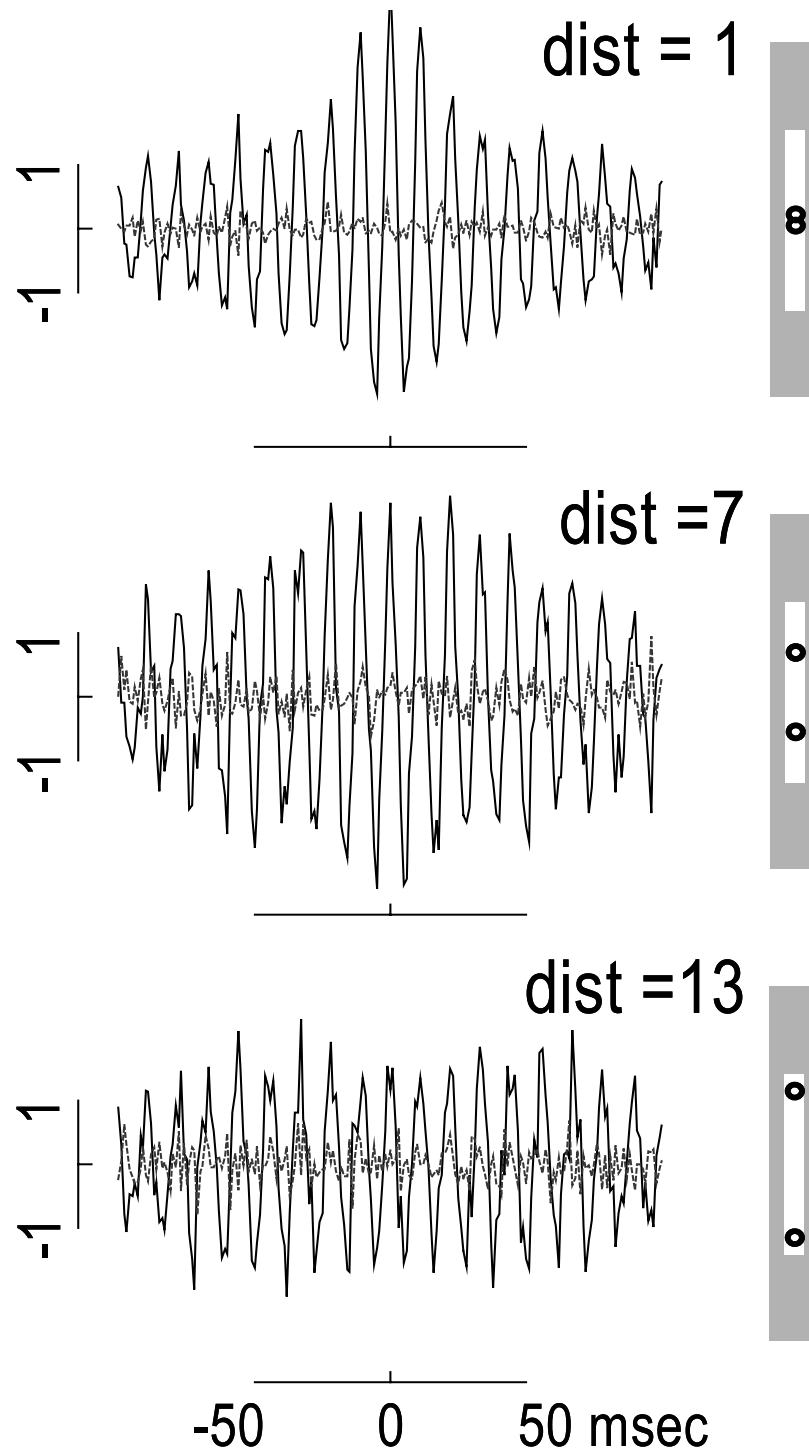


Figure 3

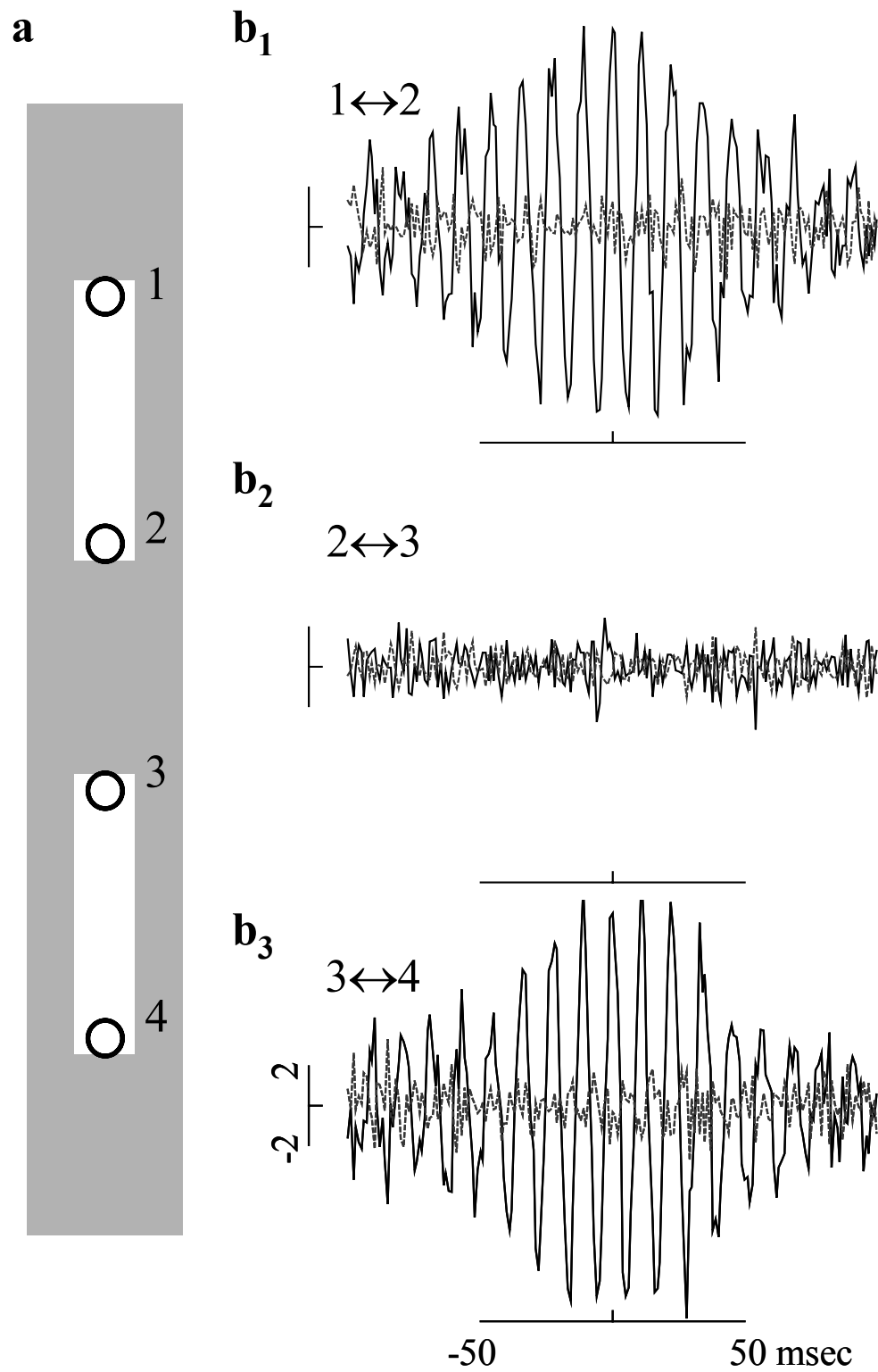


Figure 4

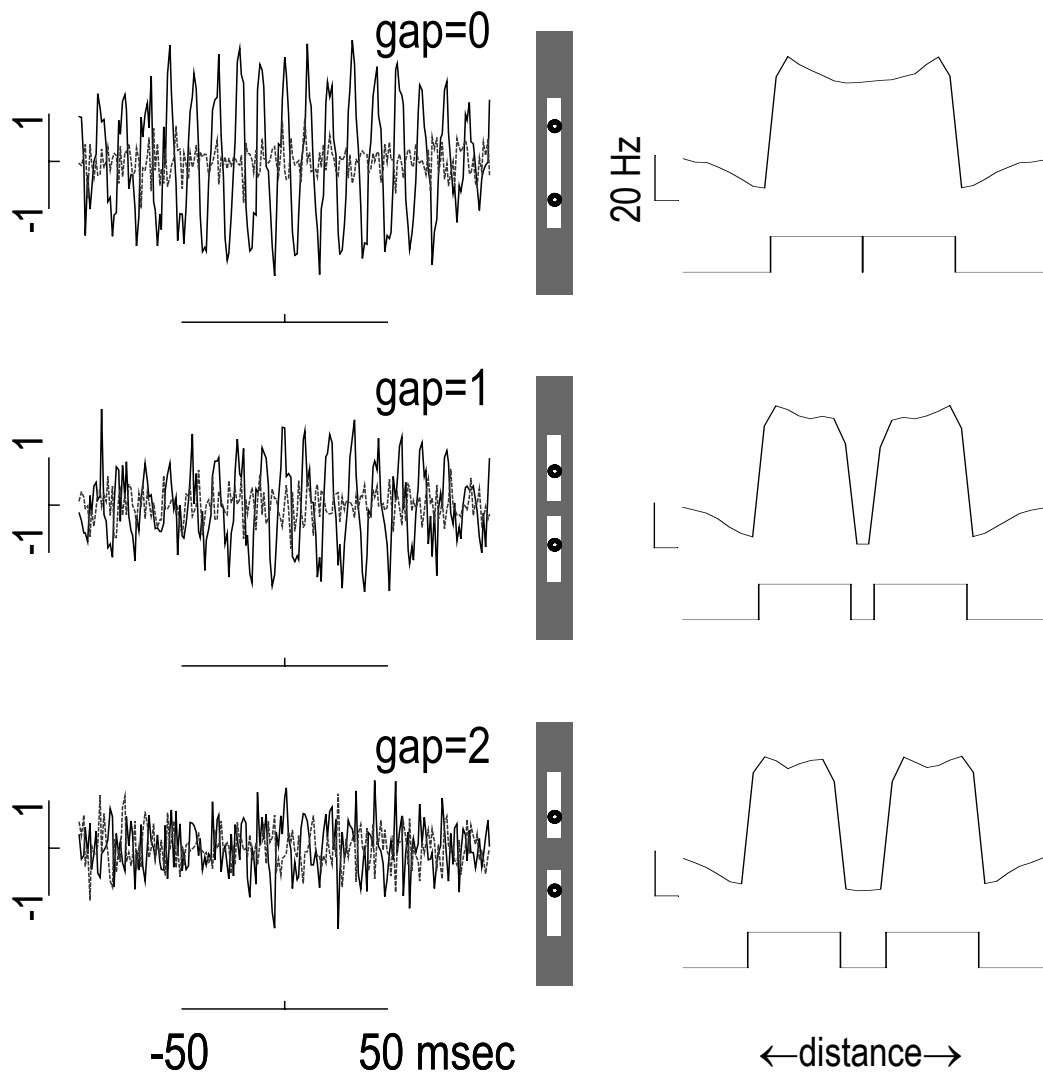


Figure 5

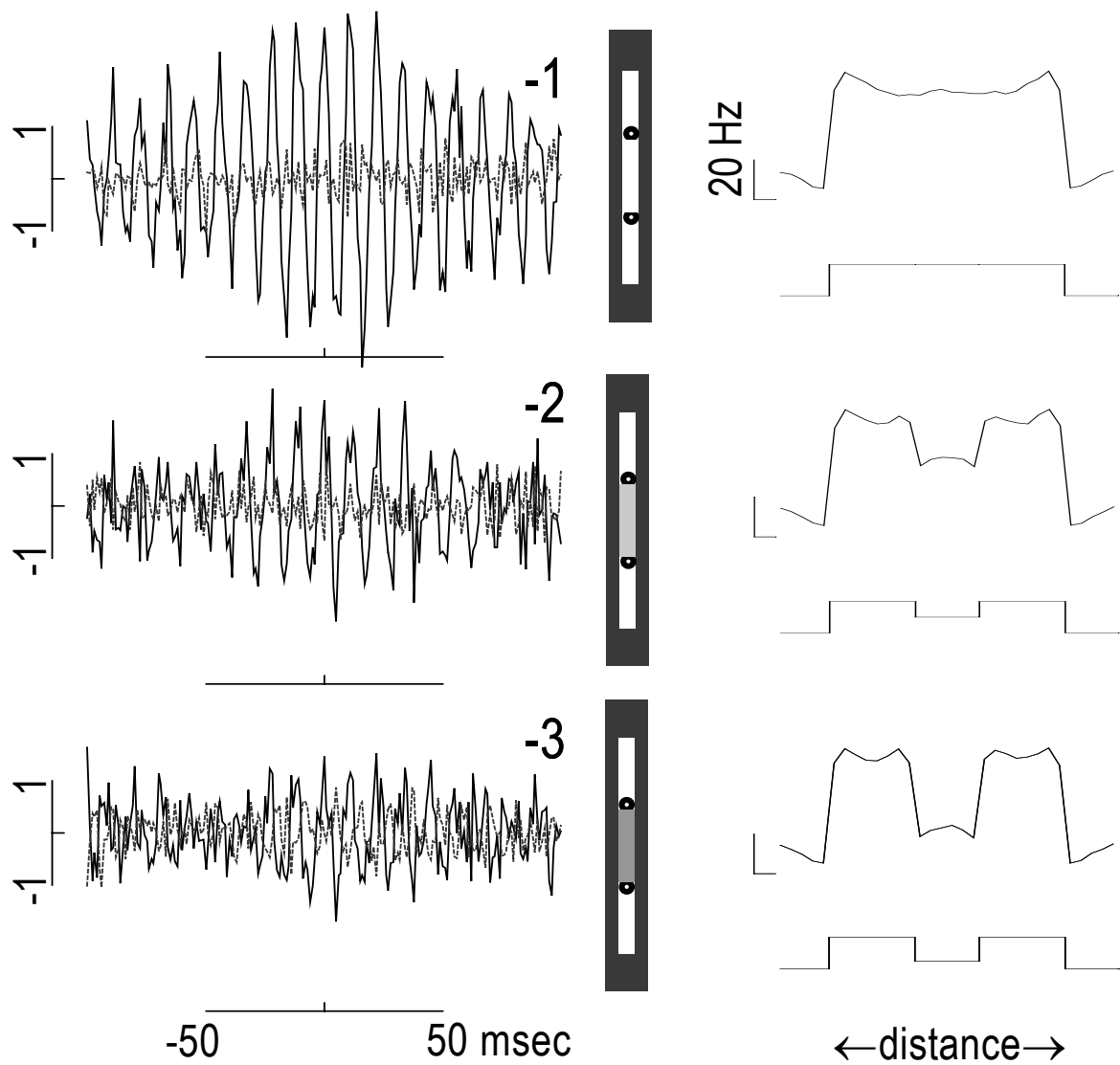


Figure 6

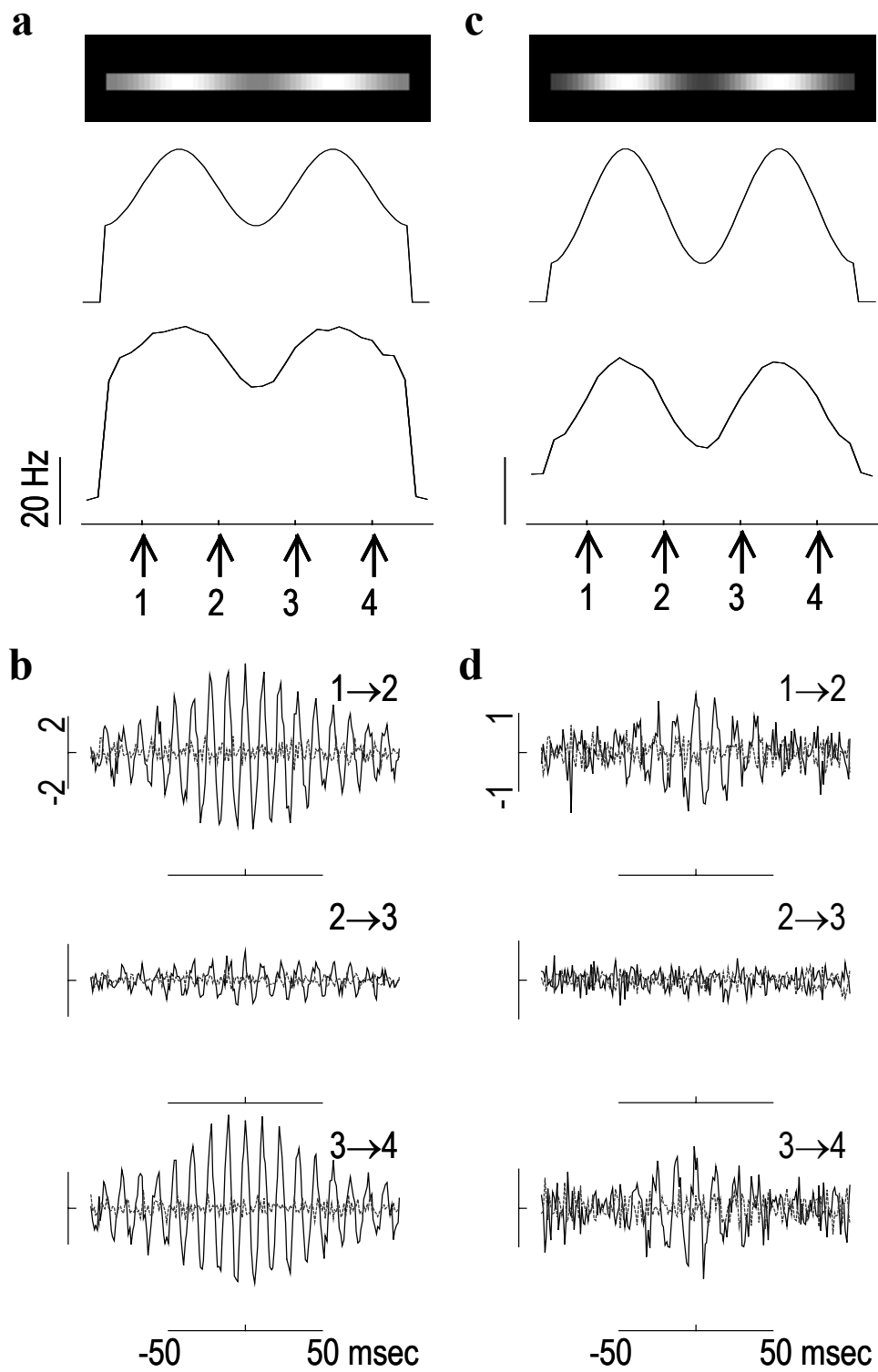


Figure 7